Structure–property relationship studies of copper(I) complexes of nanosized hypodentate ligands and evaluation of their antitumor and antimicrobial activities

Amel F. ElHusseiny, Ali Eldissouky, Ahmed M. Al-Hamza & Hammed H.A.M. Hassan

View supplementary material

Submit your article to this journal

View related articles

Citing articles: 1 View citing articles

Accepted author version posted online: 31 Oct 2014.
Published online: 27 Nov 2014.

Article views: 67

View Crossmark data

Taylor & Francis
Taylor & Francis Group

Structure–property relationship studies of copper(I) complexes of nanosized hypodentate ligands and evaluation of their antitumor and antimicrobial activities

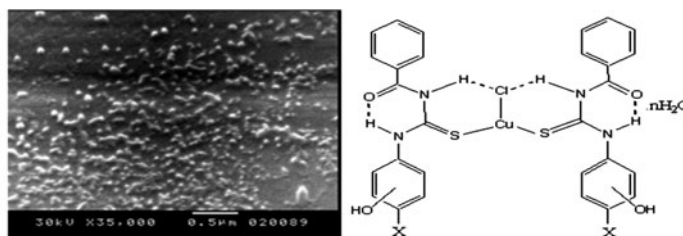AMEL F. ELHUSSEINY*, ALI ELDISSOUKY, AHMED M. AL-HAMZA and
HAMMED H.A.M. HASSAN

Faculty of Science, Chemistry Department, Alexandria University, Alexandria, Egypt

We report the preparation of four nanosized isomers of *N*-benzoyl-*N*′-(hydroxyphenyl) thioureas by nanoprecipitation. Direct reactions with $CuCl_2 \cdot 2H_2O$ gave the corresponding complexes in good yields. The structures of the ligands and their copper complexes were characterized using different analytical and spectroscopic measurements. In all complexes, the data revealed non-electrolytic mononuclear three-coordinate copper(I) complexes, where the ligand is hypodentate to copper ion via thioamide sulfur. Thermal studies revealed high thermal stability of the complexes compared to their parent ligands and the mechanism of decomposition and the thermodynamic parameters were evaluated. The ligands and their complexes were screened against different pathogenic microorganisms, and subjected to *in vitro* antioxidant and cytotoxic activities against three human cell lines. Compared to other isomers, *N*-benzoyl-*N*′-(*o*-hydroxyphenyl) thiourea exhibited significant antimicrobial activity and had higher activity than the standard fungicides and bacteriocides. All copper complexes showed inhibitory potencies, however $[Cu(H_2L^2)_2Cl]$ exhibited remarkable inhibitory activities against the examined cancer cell lines as evident by the range of IC_{50} values (4.0–7.4 μg/mL) and the percentage of cell viability. The results obtained can find medical applications as new therapeutic nanoparticle agents.

Keywords: Hypodentate ligands; Copper(I) complexes; Thermal analyses; Cytotoxic activity

1. Introduction

Metal complexes of hypodentate ligands have importance in design and synthesis of hetero-polymetallic systems [1] due to their applications in metal separation and extraction [2],

---

*Corresponding author. Email: amel_elhusseiny@sci.alexu.edu.eg

precursors for nanomaterials [3], and biological activities [4]. *N*-benzoyl-*N*′-arylthioureas have at least three potential donors (N, O, and S) and have been regarded as model compounds for different intra and intermolecular interactions involving sulfur [5]. Hypodentate coordination only through sulfur as neutral, monodentate ligand is seen in some Au(I) [6], Ag(I) [7], Hg(II) [8], Pt(II) [9], and Cu(I) [10] complexes. Such ligands form intramolecular H-bonds between the oxygen of C=O and hydrogen of thiourea [11] forming a stable six-membered ring [12]. For this reason, the hydrogen-bonding ability of the thiourea is used in construction of anion receptors [13], thiourea-based metal complexes [14], and organo catalysts [15].

Copper is an essential trace metal that has been used for centuries either as copper ions or in complexes to disinfect liquids, solids, and human tissues [16]. Copper complexes have been extensively utilized in DNA cleavage for generation of activated oxygen species by redox cycling properties between Cu(II) and Cu(I), presumably a hydroxyl radical, which can react at several nucleic acid sites to break it [17]. Many reports demonstrated that thiourea derivatives exhibit interesting biological [17, 18] and anticancer activities [19] that are enhanced by complexation with copper. In addition, there are several metal complexes that actively and specifically inhibit the chymotrypsin-like activity of the proteasome *in vitro* and in human tumor-cell cultures [20]. This is because the ubiquitin/proteasome system plays an important role in degradation of cellular proteins, and metal complexes inhibit the proteasome activity in tumor cells in 15 min [21].

In this article, we report the preparation of four nanosized isomers of *N*-benzoyl-*N*′-(hydroxylphenyl) thioureas (**H₂L¹**–**H₂L⁴**) using nanoprecipitation. Although *N*-benzoyl-*N*′-(*m*-hydroxyphenyl) thiourea and *N*-benzoyl-*N*′-(*p*-hydroxyphenyl) thiourea were previously studied by X-ray diffraction [22, 23], no report on the chemistry of nanosized *N*-benzoyl-N′-(hydroxyphenyl) thiourea was published. The application of nanomaterials to medical problems has already demonstrated a clinical impact in terms of delivery strategies for a range of bioactive molecules including therapeutic agents, nucleic acids, and imaging contrast agents [24]. These nanomaterials are used to synthesize a series of copper complexes and study their bactericidal, fungicidal, and antioxidant activities. The *in vitro* cytotoxicity against three human cell lines, liver carcinoma (HEPG2), breast carcinoma (MCF7), and colon carcinoma (HCT116) have also been evaluated.

2. Experimental

2.1. *Materials and physical measurements*

Benzoyl chloride, ammonium thiocyanate, *o*-aminophenol, *m*-aminophenol, *p*-aminophenol, and 2-amino-5-nitrophenol were purchased from Aldrich. Acetonitrile (BDH-PROLABO), ethanol, 1,4-dioxane (Aldrich), dimethylsulfoxide (DMSO, Aldrich), and diethyl ether were of analytical grade quality and used without purification. CuCl₂·2H₂O was purchased from Aldrich and used as received. Melting points were determined with an electro-thermal melting point apparatus and are not corrected. Infrared spectra (IR, KBr pellets; 3-mm thickness) were recorded on a *Perkin–Elmer* Infrared Spectrophotometer (FTIR 1650). All spectra were recorded from 4000 to 500 cm⁻¹, at 25 °C. Absorption spectra were measured with a *UV 500* UV–vis spectrometer, at room temperature in DMSO. ESR measurements on polycrystalline samples were measured at 298 K using a Varian E–12 spectrometer and DPPH as an external standard. ¹H NMR spectra were recorded on a JEOL 500 spectrometer

in DMSO-d^6 solution with TMS as internal standard. The molar conductivity measurements were carried out using an HI 8033 HANNA conductometer at 25 °C for 10^{-3} M solution in DMSO-d^6. Thermal analyses were carried out from 25 to 700 °C or 1000 °C in a stream of nitrogen by a *Shimadzu DTG 60H* thermal analyzer. The experimental conditions were: platinum crucible, nitrogen atmosphere with a 30 mL/min flow rate, and a heating rate 20 °C/min at Cairo University. Elemental analyses were performed at the Regional Center of Mycology and Biotechnology, El-Azhar University, Cairo. Metal analysis was determined by atomic absorption technique and by energy-dispersive X-ray spectroscopy (EDX) (Module Oxford 6587INCA x-sight) attached to JEOLJSM-5500LV scanning electron microscopy (SEM) at 20 kV after gold coating using SPI-Module sputter coater) at the E-Microscope Unit, Faculty of Science, Alexandria University. The morphologies of nanoparticles were observed by SEM (JEOL-JSM5300) at the E-Microscope Unit, Faculty of Science, Alexandria University. The samples were sonicated in de-ionized water for 5 min and deposited onto carbon-coated copper mesh and allowed to air-dry before examination. Cytotoxicity and antioxidant studies were performed at the Regional Center of Mycology and Biotechnology, El-Azhar University, Cairo. Antimicrobial screening tests were conducted at Faculty of Science, Alexandria University.

2.2. Synthesis of H_2L^1–H_2L^4 (General method)

H_2L^1–H_2L^4 were prepared according to the reported procedure [25]. A solution of benzoyl chloride (5 g, 35 mM) in acetonitrile (30 mL) was added dropwise to a solution of ammonium thiocyanate (2.66 g, 35 mM) in acetonitrile (30 mL) and kept in an ice bath with stirring for 1 h. The white precipitate of ammonium chloride was removed by filtration. A solution of the appropriate amino phenol, *o*-amino phenol, *m*-aminophenol, *p*-aminophenol, and 2-amino-5-nitrophenol (35 mM) in acetonitrile (30 mL) was added to the filtrate and the mixture was stirred, at room temperature for 4 h. The resulting precipitate was filtered, washed thoroughly with acetonitrile followed by diethyl ether, and then dried in a vacuum desiccator.

N-benzoyl-*N*′-(*o*-hydroxyphenyl) thiourea (**H_2L^1**): Yield: 75%. Color: yellow. Anal Found (Calcd for $C_{14}H_{12}N_2SO_2$, 272.32): C, 61.31 (61.75); H, 4.80 (4.44); N, 9.99 (10.29); S, 12.09 (11.77).

N-benzoyl-*N*′-(*m*-hydroxyphenyl) thiourea (**H_2L^2**): Yield: 75%. Color: white. Anal Found (Calcd for $C_{14}H_{12}N_2SO_2$, 272.32): C, 61.40 (61.75); H, 4.14 (4.44); N, 9.83 (10.29); S, 11.50 (11.77).

N-benzoyl-*N*′-(*p*-hydroxyphenyl) thiourea (**H_2L^3**): Yield: 75%. Color: violet. Anal Found (Calcd for $C_{14}H_{12}N_2SO_2$, 272.32): C, 62.02 (61.75); H, 4.70 (4.44); N, 10.59 (10.29); S, 11.43 (11.77).

N-benzoyl-*N*′-(2-hydroxy-4-nitrophenyl) thiourea (**H_2L^4**): Yield: 88%. Color: yellow. Anal Found (Calcd for $C_{14}H_{11}N_3SO_4$, 317.32): C, 53.36 (52.99); H, 3.17 (3.49); N, 12.60 (13.24); S, 9.71 (10.10).

2.3. Synthesis of nanosized ligands (General method)

Benzoyl chloride (1 g, 7.0 mM) dissolved in acetonitrile (50 mL) was added to (0.53 g, 7.0 mM) ammonium thiocyanate dissolved in 50-mL acetonitrile. The solution was kept in an ice bath for 1 h, filtered, and the precipitate was further washed with additional 10 mL

of acetonitrile. To the appropriate aminophenol (7.0 mM) dissolved in acetonitrile/water (110 mL) (100 mL acetonitrile and 10 mL distilled water), the filtrate was added in one portion and the resulting mixture was ultrasonicated for 3 h at 42 kHz. Centrifugation of the mixture for 15 min. at 6000 rpm produced the required ligand nanoparticles as solid products. The products were washed successively using EtOH followed by Et_2O and dried in a vacuum oven at 60 °C.

2.4. *Synthesis of copper complexes*

A warm ethanol solution (15 mL) of $CuCl_2 \cdot 2H_2O$ (0.85 g, 5.0 mM) was added to 10.0 mM of the appropriate ligand **H_2L^1–H_2L^4** in the same solvent (20 mL). The mixture was refluxed for 2 h and the precipitate formed in each case was collected by filtration, washed thoroughly with ethanol followed by Et_2O, and dried in a vacuum oven at 60 °C.

[$Cu(H_2L^1)_2Cl$]·$2H_2O$: Yield: 70%. Color: greenish black. Anal Found (Calcd for $CuC_{28}H_{28}N_4S_2O_6Cl$, 679.64): C, 49.82 (49.44); H, 4.43 (4.12); N, 8.60 (8.24); S, 9.75 (9.42); Cu, 9.29 (9.34).

[$Cu(H_2L^2)_2Cl$]: Yield: 68%. Color: yellowish green. Anal Found (Calcd for $CuC_{28}H_{24}N_4S_2O_4Cl$, 643.64): C, 52.53 (52.20); H, 4.01 (3.73); N, 8.61 (8.70); S, 9.66 (9.95); Cu, 10.00 (9.86).

[$Cu(H_2L^3)_2Cl$]·$2H_2O$: Yield: 55%. Color: greenish black. Anal Found (Calcd for $CuC_{28}H_{28}N_4S_2O_6Cl$, 679.64): C, 49.52 (49.44); H, 3.50 (4.12); N, 8.60 (8.24); S, 9.41 (9.42); Cu, 9.22 (9.34).

[$Cu(H_2L^4)_2Cl$]: Yield: 75%. Color: yellowish green. Anal Found (Calcd for $CuC_{28}H_{22}N_6S_2O_8Cl$ 733.64): C, 45.83 (45.80); H, 3.00 (3.00); N, 11.63 (11.45); S, 8.70 (8.72); Cu, 8.60 (8.65).

2.5. *Biological activity*

2.5.1. *In vitro* cytotoxicity screening. The mammalian cell lines: liver carcinoma cell lines (HEPG2), breast carcinoma cell line (MCF7), and colon carcinoma cell line (HCT116) were obtained from VACSERA Tissue Culture Unit. Chemicals used: DMSO, crystal violet, and trypan blue dye were purchased from Sigma (St. Louis, MO, USA). Fetal bovine serum, DMEM, RPMI-1640, HEPES buffer solution, L-glutamine, gentamycin, and 0.25% Trypsin–EDTA were purchased from Lonza. Crystal violet stain (1%) is prepared from 0.5% (w/v) crystal violet and 50% ethanol, diluted with distilled water then filtered through a Whatman filter paper No.1. Cell lines propagation: the cells were propagated in Dulbecco's modified Eagle's medium (DMEM) supplemented with 10% heat-inactivated fetal bovine serum, 1% L-glutamine, HEPES buffer, and 50-μg/mL gentamycin. All cells were maintained at 37 °C in a humidified atmosphere with 5% CO_2 and were subcultured twice a week. Cell toxicity was monitored by determining the effect of the test samples on cell morphology and cell viability. For cytotoxicity assay, the cells were seeded in a 96-well plate at cell concentration of 1×10^4 cells per well in 100 μL of growth medium. Fresh medium containing different concentrations of the test sample was added after 24 h of seeding. Serial twofold dilutions of the tested chemical compound were added to confluent cell monolayers dispensed into 96-well, flat-bottomed microliter plates (Falcon, Nu, USA) using a multichannel pipette. The microliter plates were incubated at 37 °C in a humidified incubator with 5% CO_2 for 48 h. Three wells were used for each concentration of the test samples.

Control cells were incubated without test sample, and with or without DMSO. The small percentage of DMSO present in the wells (maximum 0.1) does not affect the experiment. After incubation of the cells for 24 h at 37 °C, various concentrations of sample (50, 25, 12.5, 6.25, 3.125, and 1.56 μg) were added and the incubation was continued for 48 h; viable cells were determined by a colorimetric method. In brief, after the end of the incubation period, media were aspirated and crystal violet solution (1%) was added to each well for at least 30 min. The stain was removed and the plates were rinsed using tap water until all excess stain is removed. Glacial acetic acid (30%) was then added to all wells and mixed thoroughly, and then the absorbance of the plates were measured after gently shaking on a Micro plate reader (TECAN, Inc.) using a test wavelength of 490 nm. All results were corrected for background absorbance detected in wells without added stain. Treated samples were compared with the cell control in the absence of the tested compounds. All experiments were carried out in triplicate. The cell cytotoxic effect of each tested compound was calculated [26, 27]. The inhibitory activity IC_{50} of the tested vinblastine standard drug against the studied carcinoma cell lines was detected under the above experimental conditions.

2.5.2. Antimicrobial activity. Antimicrobial activities of the tested samples were determined using a modified Kirby–Bauer disk diffusion method [28]. All the synthesized compounds were dissolved to prepare a stock solution of 1 mg/mL in DMSO. Stock solution was aseptically transferred and twofold diluted to have solutions of different concentrations. The antibacterial and antifungal activities of test compounds were done by paper disk method [29] and the activities were determined by measuring the diameters of the inhibition zone (mm). Media with DMSO was set up as control. All cultures were routinely maintained on nutrient agar (NA) and incubated, at 37 °C. The inoculums of bacteria were performed by growing the culture in NA broth at 37 °C overnight. Approximately 0.1 mL of diluted bacterial or fungal culture suspension was spread with the help of a spreader on NA plates uniformly. Solutions of the tested compounds and reference drugs were prepared by dissolving 10 mg of the compound in 10-mL DMF. A 100-μL volume of each sample was pipetted into a hole (depth 3 mm) made in the center of the agar. Sterile 8-mm disks (Himedia Pvt. Ltd.) were impregnated with test compounds. The disk was placed onto the plate. Each plate had one control disk impregnated with solvent. The plates were incubated at 37 °C for 18–48 h. Standard disks of Tetracycline and Streptomycin (Antibacterial agents; 10 μg/disk) and Amphotericin B (Antifungal agent; 10 μg/disk) served as positive controls for antimicrobial activity, while filter disks impregnated with 10 μL of DMSO were used as a negative control.

3. Results and discussion

3.1. *Synthesis and characterization*

Nanosized aromatic compounds could be obtained by either emulsion or interfacial methods. A popular method used for such nanosized preparation is solvent displacement, also referred to as nanoprecipitation [30]. The basic principle of this technique is based on the interfacial deposition of a product after displacement of a semi-polar solvent, miscible with

water, from a lipophilic solution. Rapid diffusion of the solvent into the non-solvent phase results in a decrease of interfacial tension between the two phases, which increases the surface area and leads to formation of small droplets of the organic solvent. The key variables determining the success of the method and affecting the physicochemical properties of nanoparticles are those associated with adding the organic phase to the aqueous phase, such as organic phase injection rate, aqueous phase agitation rate, the method of organic phase addition, and the organic phase to aqueous phase ratio. Likewise, nanoparticle characteristics are influenced by the nature and concentration of their components [31]. The process of particle formation in the nanoprecipitation method comprises three stages: nucleation, growth, and aggregation. The rate of each step determines the particle size and the driving force of these phenomena is the ratio of product concentration over the solubility of the product in the solvent mixture. The separation between the nucleation and the growth stages is the key factor for uniform particle formation [32].

The nanosized *N*-benzoyl-*N′*-(*o*-hydroxyphenyl) thiourea H_2L^1, *N*-benzoyl-*N′*-(*m*-hydroxyphenyl) thiourea H_2L^2, *N*-benzoyl-*N′*-(*p*-hydroxyphenyl) thiourea H_2L^3, and *N*-benzoyl-*N′*-(2-hydroxy-4-nitrophenyl) thiourea H_2L^4 were prepared by reaction of benzoyl chloride dissolved in acetonitrile with ammonium thiocyanate dissolved in the same solvent (scheme 1). After removing the white precipitate of ammonium chloride, the filtrate was added in one portion to the appropriate aminophenol, namely *o*-amino phenol, *m*-aminophenol, *p*-aminophenol, and 2-amino-5-nitrophenol dissolved in acetonitrile/water mixture (10 : 1). Ultra sonication followed by centrifugation furnished the targeted adducts. The
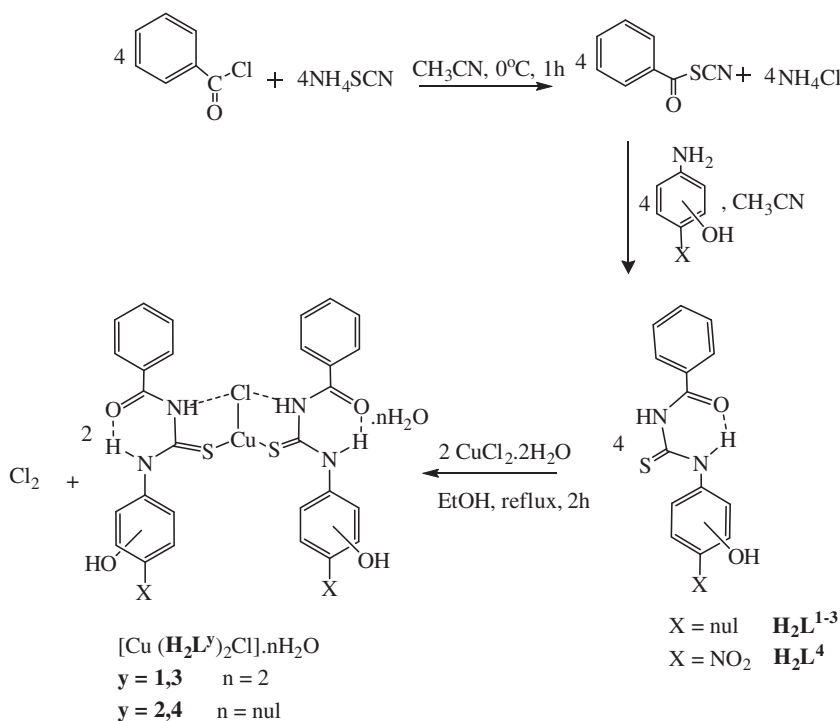
Scheme 1.   Synthesis of free H_2L^1–H_2L^4 and their copper complexes.

Table 1. Characterization data of $\mathbf{H_2L^1}$–$\mathbf{H_2L^4}$ and their copper(I) complexes.

Compound (formula)	$\Lambda_M{}^a$	^{1}H-NMR δ (ppm)	^{13}C-NMR δ (ppm)	IR (KBr) υ (cm^{-1})	λ_{max} (nm)
$\mathbf{H_2L^1}$		12.94 (1H, NH), 11.43 (1H, NH), 10.19 (1H, OH), 8.50–6.81 (9H, Ar)	176.22 (C=S), 165.48 (C=O)	3303, 3261, 3035, 1655, 1560, 1372, 1257, 1197, 929	279
[Cu(H$_2$L^1)$_2$Cl]·2H$_2$O	2.2	12.10 (2H, 2NH), 11.43 (2H, 2NH), 10.50 (2H, 2OH), 7.50–7.00 (18H, Ar)		3378, 3270, 3185, 1676. 1537, 1251, 1397, 1185, 904	281
$\mathbf{H_2L^2}$		12.62 (1H, NH), 11.48 (1H, NH), 9.64 (1H, OH), 7.93–6.75 (9H, Ar)	179.08 (C=S), 168.86 (C=O)	3327, 3225, 3125, 1673. 1527, 1262, 1329, 1143, 994	270
[Cu(H$_2$L^2)$_2$Cl]	2.0	12.52 (2H, 2NH), 11.44 (2H, 2NH), 9.68 (2H, 2OH), 8.13–7.01 (18H, Ar)		3371, 3271, 3055, 1676, 1533, 1385,1259, 1144, 977	278
$\mathbf{H_2L^3}$		11.0 (1H, NH), 10.01 (1H, NH), 9.91 (1H, OH), 8.01–6.73 (9H, Ar)	(177.89) (C=S), (165.58) (C=O)	3328, 3235, 3058, 1649, 1539, 1363, 1224, 1170, 983	282
[Cu(H$_2$L^3)$_2$Cl]·2H$_2$O	1.2	12.73 (2H, 2NH), 12.44 (2H, 2NH), 9.69, 9.59 (2H, 2OH), 8.09–5.80 (18H, Ar)		3303, 3262, 3062, 1265, 1665, 1537, 1335, 1216, 925	280
$\mathbf{H_2L^4}$		13.3 (1H, NH), 11.76 (1H, NH), 11.5 (1H, OH), 8.07–6.95 (9H, Ar)	(178.64) (C=S), (169.04) (C=O)	3395, 3247, 2996, 1657, 1520, 1338, 1260 1193, 955	286
[Cu(H$_2$L^4)$_2$Cl]	1.4	11.52 (2H, 2NH), 11.27 (2H, 2NH), 10.04 (2H, 2OH), 8.39–6.61 (18H, Ar)		3390, 3225, 3156, 1665, 1569, 1347, 1285, 1173, 934	283

$^a\Lambda_M$ = molar conductance in 10^{-3} M DMSO in (Ω^{-1} cm^2 mol^{-1}).

structures of the prepared ligands were fully characterized by different analytical methods, including FTIR, UV–visible, NMR table 1, and elemental analyses (see section 2).

As judged by SEM photographs (figure 1), the average diameter of the particles ranges from 26 to 153 nm and interconnection between particles was present in a greater or lesser extent. The average diameter of the particles was estimated from SEM images and selected at random. The average diameters of $\mathbf{H_2L^1}$, $\mathbf{H_2L^2}$, $\mathbf{H_2L^3}$, and $\mathbf{H_2L^4}$ were 26, 67, 90, and 153 nm; standard deviations were 6.72, 21.11, 8.07, and 2.72, respectively. $\mathbf{H_2L^1}$, $\mathbf{H_2L^2}$, and $\mathbf{H_2L^4}$ were obtained as well-separated spherical nanoparticles with some interconnection. However, high degree of interconnection between the particles was found in $\mathbf{H_2L^3}$. Based on these results, it is possible to conclude that addition of a particular amount of water to the reaction system was essential for formation of spherical particles and to control the degree of interconnection. The tendency of spherical particle formation of such isomeric *N*-benzoyl-*N'*-(hydroxyphenyl) thioureas may be correlated to the dispersion stability of particles in the reaction solution or the precipitation mechanism of the particles.

Reaction of equimolar amounts of the ligands with copper(II) chlorides furnished the corresponding copper complex [Cu(H$_2$L$^{1-4}$)$_2$Cl]·nH$_2$O, where n = 0 or 2 (scheme 1). For structural elucidations and comparison purposes, bulk production of free $\mathbf{H_2L^1}$–$\mathbf{H_2L^4}$ was considered [25]. Analytical, energy-dispersive X-ray spectroscopy (EDX) (figure 2), molar conductance, and spectral studies reveal that the obtained complexes are non-electrolytes and contain two ligand molecules in addition to one chloride. The complexes are air-stable,
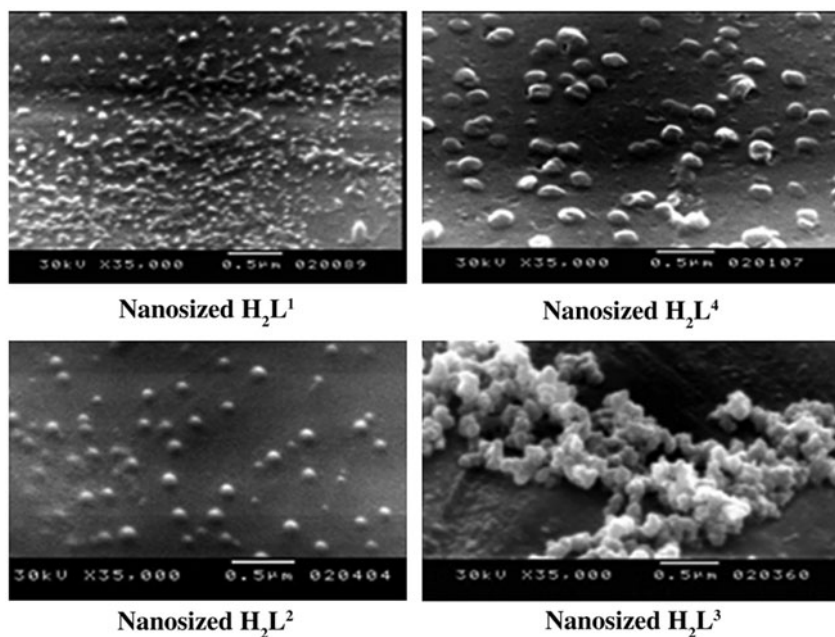
Figure 1. SEM images of the nanosized H_2L^1–H_2L^4.

non-hygroscopic, and soluble in both DMSO and DMF. Table 1 compiles the spectral data of H_2L^1–H_2L^4 and their copper complexes $Cu(H_2L^1)_2(Cl)\cdot2H_2O$, $Cu(H_2L^2)_2(Cl)$, $Cu(H_2L^3)_2(Cl)\cdot2H_2O$, and $Cu(H_2L^4)_2(Cl)$, in addition to the molar conductivity data of the copper complexes.

The higher affinity of sulfur to Cu^{+1} seems to play a role in the reduction of Cu(II) to Cu (I). A plausible explanation is that the synthesized benzoyl thiourea derivative may be oxidized to disulfide and Cu^{+2} is reduced to Cu^{+1} which remains in solution as a complex with acetonitrile [33]. At the same time, intramolecular hydrogen bonds of the type NH···Cl may be assumed to contribute to the stabilization of the Cu(I) complexes [34].

3.1.1. FTIR Spectroscopy. The main bands of FTIR spectra of H_2L^1–H_2L^4 and their copper complexes are given in table 1. The FTIR spectra of free H_2L^1–H_2L^4 display bands at $v3395$–3303, $v3261$–3225, $v3185$–3125, $v3062$–3035, $v1673$–1649, $v1560$–1520 and $v1285$–1251 cm^{-1} assigned to v(OH), v(N–H), v(N′–H), v(CH), v(C=O), δ(N′–H, thioamide band I), and v(C=S), respectively. The assignment of v(N–H) above 3200 cm^{-1} while v(N′–H) above $v3000$ cm^{-1} could be referred to the intramolecular hydrogen bonding of the form N′–H…O=C and the possibility of *trans–cis* conformation of benzoyl thiourea which affects the vibrational positions and properties of the central –C(O)NHC(S)N′H- moiety [23, 12, 35]. The intramolecular hydrogen bond between oxygen in C=O and hydrogen of thiourea forms a six-membered ring which can stabilize the molecular conformation of the prepared compounds [11, 12]. The lack of v(SH) around 2500–2600 cm^{-1} indicated the absence of the v(N=C-SH) tautomeric form and H_2L^1–H_2L^4 remain in the thioketo-amine form [36].
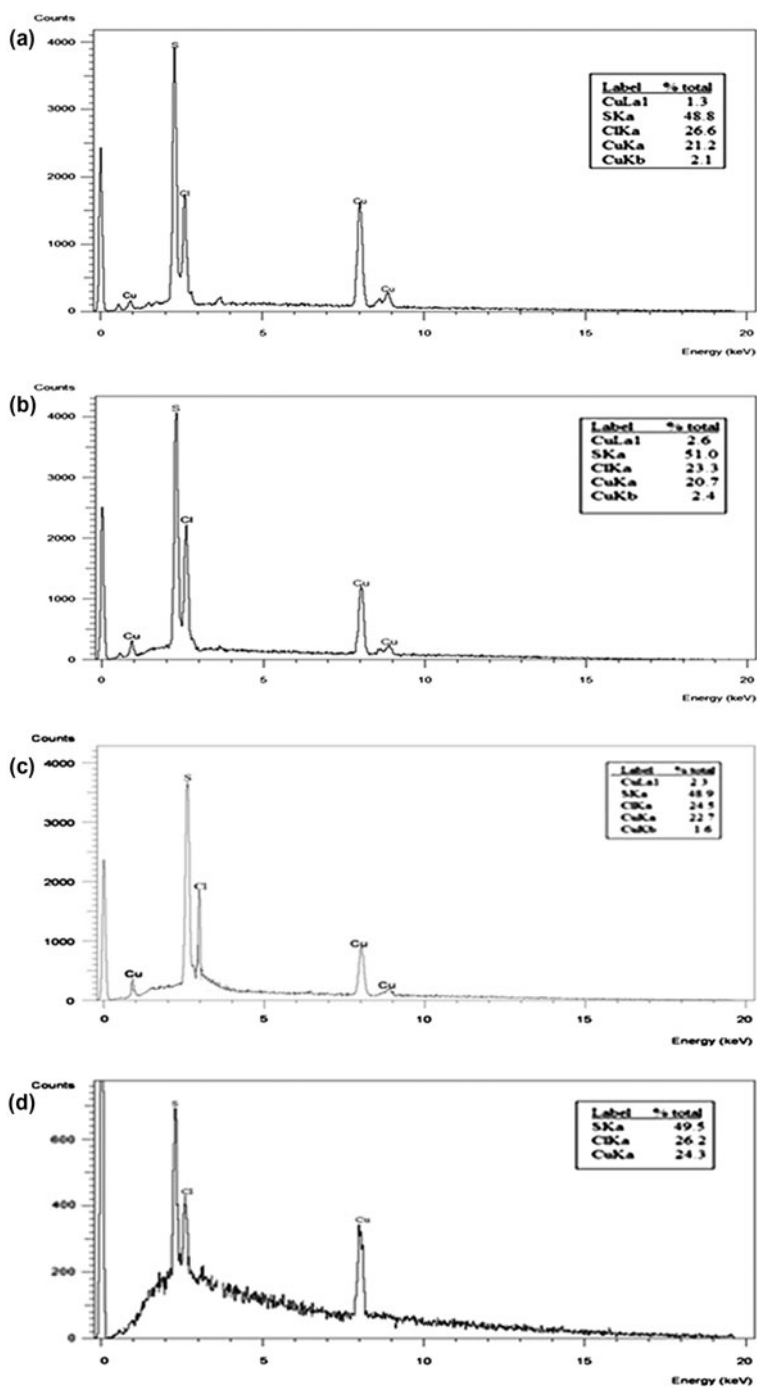
Figure 2. EDX for (a) $[Cu(H_2L^1)_2(Cl)]\cdot 2H_2O$, (b) $[Cu(H_2L^2)_2(Cl)]$, (c) $[Cu(H_2L^3)_2(Cl)]\cdot 2H_2O$, and (d) $[Cu(H_2L^4)_2(Cl)]$.

The bands at ν1143–1197 cm^{-1}, ν1329–1372 cm^{-1}, and ν928–994 cm^{-1} in spectra of the free ligands are assigned to ν_{asym}(NCN′) thioamide band II, ν_{sym}(NCN′) thioamide band III, and thioamide band IV, respectively [37–40]. The ν(C=O) is at relatively lower value than ordinary carbonyl absorption (1700 cm^{-1}) attributed to the intramolecular hydrogen bond and to the conjugated resonance interactions between the carbonyl and the phenyl ring in *N*-benzoyl substituted thiourea compounds [34, 38–40]. The band at ν1520 cm^{-1} in spectra of H_2L^4 is assigned to ν(NO$_2$). The FTIR spectral data of copper complexes (table 1) demonstrate a shift of ν(C=S) to lower wavenumbers compared to the free ligands, suggesting participation of sulfur of the thioamide group in coordination [35]. The coordination of S of the thiourea derivative with metal ions causes a charge transfer ligand–metal which reduces the double bond character of the C=S bond and allows a lower frequency shift of thioimide band (IV). The shift of ν(OH) and ν(NH) to higher wavenumber compared to the parent ligands ruled out their involvement in coordination. In all copper complexes, the value of νC=O remains unchanged or upward shifted indicating its non-bonding nature [39, 40].

3.1.2. Electronic spectra. Electronic spectra of H_2L^1–H_2L^4 and their copper complexes in DMSO are collected in table 1. The electronic spectra of free H_2L^1–H_2L^4 exhibited one band at λ269–280 nm due to intraligand π–π* transition [40]. The observed band at λ278–283 nm assigned to ligand centered π–π* transitions show a small red shift as a consequence of coordination to copper. The ESR spectra of the polycrystalline copper complexes did not exhibit any signal characteristic of copper(II) confirming the formation of copper(I) complexes.

3.1.3. NMR Spectroscopy. NMR spectral data of H_2L^1–H_2L^4 in DMSO-d$_6$ are compiled in table 1. ^{1}H NMR spectra of H_2L^1 displayed the expected functional group signals at δ12.94 ppm (thioamide), δ11.43 ppm (amide), and δ10.19 ppm (OH), respectively, while the nine aromatic protons resonated at δ6.81–8.50 as a multiplet. Similarly, H_2L^2 displayed signals at δ12.62 ppm (thioamide), δ11.48 ppm (amide), δ9.64 ppm (OH), and the nine aromatic protons as multiplets at δ6.75–7.93 ppm. H_2L^3 exhibited signals at δ11.00 ppm (thioamide), δ10.01 ppm (amide), δ9.91 ppm (OH), and the nine aromatic protons as a multiplet at δ6.73–8.01 ppm. H_2L^4 showed signals at δ13.30 ppm (thioamide), δ11.76 ppm (amide), δ11.50 ppm (OH), and the eight aromatic protons as a multiplet at δ6.95–8.07 ppm. The low field positions of most signals may be taken as evidence for different hydrogen bonding participation such as intramolecular NH–O=C- [12, 13], intermolecular OH···DMSO, intermolecular DMSO···HN-C=S, or intermolecular hydrogen bonding between the ligand molecules. The deshielding of NH and OH signals in H_2L^4 could be attributed to the presence of NO$_2$. Moreover, thioamide protons in H_2L^1–H_2L^3 are downfield shifted in the order *o*-OH > *m*-OH > *p*-OH due to intramolecular H-bonding.

^{1}H-NMR spectra of the copper complexes in DMSO-d$_6$ are very useful in determining coordination between the prepared benzoyl thioureas and copper ions. From table 1, it is clear that an appreciable change occurs in the position of the thioamide signal of H_2L^1, H_2L^2 and H_2L^4 upon complex formation. The thioamide proton signal in [Cu(H$_2L^1$)$_2$Cl]·2H$_2$O, [Cu(H$_2L^2$)$_2$Cl], and [Cu(H$_2L^4$)$_2$Cl] is upfield shifted relative to their parent ligands. This shift is attributed to the participation of the thioamide in bonding to the copper ion, and thus further confirms the FTIR data. The thioamide proton signal in case of

$[Cu(H_2L^3)_2Cl] \cdot 2H_2O$ was observed at $\delta 12.73$ ppm compared to $\delta 11.00$ ppm in case of the free ligand. This downfield shift could be attributed to deshielding resulting from bonding to copper ion. The amide proton signals at $\delta 10.01$–11.76 ppm in the free ligands did not exhibit appreciable change for $[Cu(H_2L^1)_2Cl] \cdot 2H_2O$ and $[Cu(H_2L^2)_2Cl]$, however, down-field shifted in case of $[Cu(H_2L^3)_2Cl] \cdot 2H_2O$ by $\Delta\delta = +2.43$ ppm resulting from H-bonding formation of the type –NH–Cl and –NH···O similar to the reported data [34]. On the other hand, the amide proton signal is upfield shifted by $\Delta\delta = -0.41$ ppm in case of $[Cu(H_2L^4)_2Cl]$ attributed to the electronic effect of the nitro group. The chemical shift of the aromatic protons of the free ligands did not show appreciable change upon complexation. The integration values of all signals indicate the bonding of two ligand molecules to the copper ion, thus confirming the micro analytical data.

In conclusion, the observed spectral data revealed that Cu(II) is reduced to Cu(I) during the course of reaction and are in agreement with the proposed molecular formulas (table 1). As a representative example for the ^{1}H-NMR spectra of the investigated compounds, figure 3 displays the ^{1}H-NMR spectrum of **H₂L¹** and its copper complex $[Cu(H_2L^1)_2Cl] \cdot 2H_2O$.
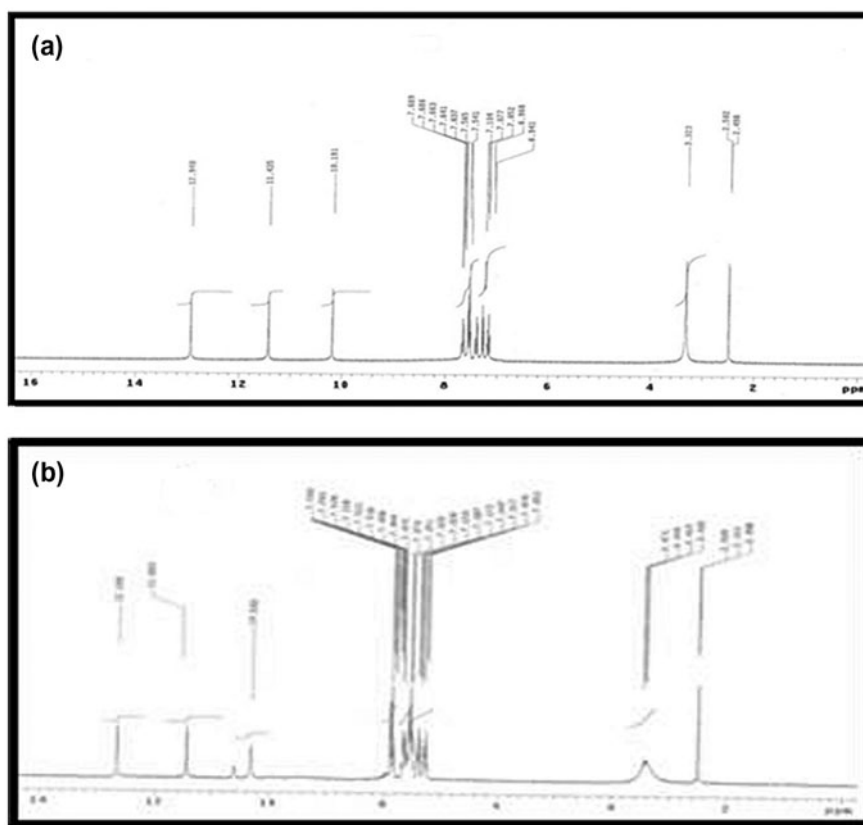
Figure 3. ^{1}H-NMR spectra of (a) **H₂L¹** and (b) $[Cu(H_2L^1)_2(Cl)] \cdot 2H_2O$.

Table 2. Thermal analysis of H_2L^1–H_2L^4 and their copper complexes.

Compounds	Decom. stages	TG (°C)	Mass loss (%) found (calculated)	DTG (°C)	DTA (°C)	Residue (%) found (calculated)
H_2L^1	I	185–700	99.23 (100)	227	227 (endo)	–
					390 (endo)	
$[Cu(H_2L^1)_2(Cl)]\cdot2(H_2O)$	I	25–389	57.62 (56.92)	339	339 (exo)	$0.5Cu_2S + S{\rightarrow}CuO + S$
	II	389–523	25.50 (25.32)	458	458 (exo)	16.82 (16.40)
H_2L^2	I	50–250	62.19 (61.39)	222	191 (endo)	–
	II	250–370	31.20 (31.98)	300	221 (endo)	
	III	370–616	6.13 (6.25)	560	580 (exo)	
$[Cu(H_2L^2)_2(Cl)]$	I	30–247	23.72 (24.23)	230	219 (endo)	$0.5Cu_2S$
	II	247–369	35.20 (34.74)	296	301 (endo)	11.50 (12.35)
	III	369–700	29.58 (27.83)	560	563 (exo)	
H_2L^3	I	35–252	54.18 (55.88)	237	200 (endo)	–
	II	252–337	31.84 (31.98)	288	240 (endo)	
	III	337–545	13.36 (12.12)	482	500 (exo)	
$[Cu(H_2L^3)_2(Cl)]\cdot2(H_2O)$	I	30–169	13.46 (13.46)	148	350 (exo)	$Cu + S$
	II	169–400	71.90 (72.39)	380	450 (exo)	14.64 (14.06)
H_2L^4	I	70–250	34.731 (33.12)	221	221 (endo)	C
	II	250–360	43.617 (43.86)	272	453 (exo)	3.63 (3.78)
	III	360–590	18.023 (18.25)	453		
$[Cu(H_2L^4)_2(Cl)]$	I	280–380	43.33 (43.20)	300	310 (endo)	56.90 (56.75)
					470 (endo)	
					500 (exo)	

3.2. *Thermal studies*

Thermal data of H_2L^1–H_2L^4 and their copper complexes were studied utilizing TGA, DTG, and DTA methods under nitrogen and the results are given in table 2. The correlation between the different decomposition steps of the compounds with the corresponding % weight losses are shown in schemes S1–S4 (see online supplemental material at http://dx.doi.org/10.1080/00958972.2014.982551), in terms of the molecular formulas of the studied compounds. As a representative example for the thermal profiles of the investigated compounds, figure 4 displays the TGA/DTA curves of H_2L^1 and its copper complex [Cu$(H_2L^1)_2$Cl]·2H_2O. The TGA curve of H_2L^1 shows one decomposition process from 185 to 700 °C with a mass loss of 99.23% (Calcd 100%). This rapid decomposition process displayed a maximum DTG peak at 227 °C. The DTA curve gave two endothermic peaks, at 227 and 339 °C, corresponding to the melting and decomposition of the ligand, respectively. The TGA profile of [Cu$(H_2L^1)_2$Cl]·2H_2O proceeds in two degradation steps over a temperature range 25–525 °C.

The mechanism of decomposition is illustrated in scheme S1 (Supplementary Material). The DTG and DTA curves pointed to the decomposition of the complex in two successive peaks at 339 and 458 °C, respectively, followed by oxidation of the metal sulfide to metal oxide [41].

The TGA curve of H_2L^2 exhibited gradual decomposition in cumulative stages from 50 to 250 °C, 250 to 370 °C, and 370 to 616 °C. The first decomposition step may attribute to loss of C_7H_7NSO fragment; weight loss 62.19% (Calcd 61.03%) and an endothermic DTA peak at 191 °C. The second decomposition step brings an endothermic peak at 221 °C which may be attributed to elimination of CO and HCNS; mass loss is 31.20% (Calcd 31.98%). The remaining part of the molecule decomposed at 580 °C. The TGA curve of
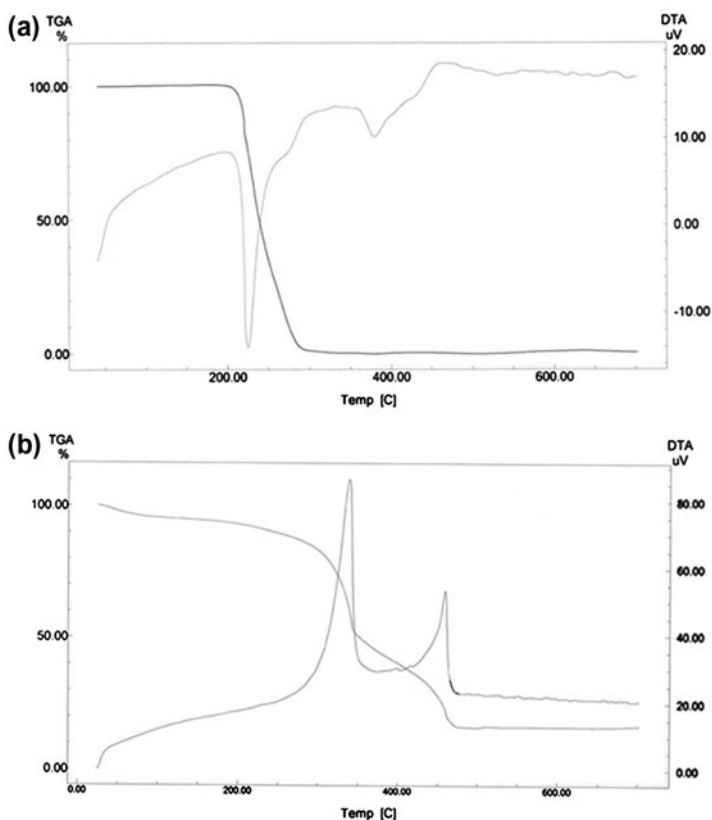
Figure 4.   The TGA/DTA curves of (a) H_2L^1 and (b) $[Cu(H_2L^1)_2Cl]\cdot2H_2O$.

$[Cu(H_2L^2)_2(Cl)]$ reveals a mass loss in three stages from 35 to 700 °C (scheme S2) (Supplementary Material). The DTA registered two endothermic peaks at 219 and 301 °C and one exothermic peak at 563 °C. The mass of the remaining residue may refer to either copper sulfide or copper oxide [42].

The TGA/DTA profile curves of H_2L^3 have three degradation steps with three well characterized DTA peaks at 200, 240, and 500 °C. The degradation steps may account for loss of C_7H_6SNO, $CO + HSCN$, and NH_2OH within estimated mass losses of 54.18% (Calcd 55.88%), 31.84% (Calcd 32.35%), and 13.36% (Calcd 12.12%), respectively. The corresponding $[Cu(H_2L^3)_2Cl]\cdot2H_2O$ complex decomposed thermally in two successive steps from 30 to 480 °C. The DTA curve displayed two exothermic peaks at 350 and 460 °C, respectively. The thermal pattern of decomposition is outlined in scheme S3 (Supplementary Material). The final decomposition step is associated with the final degradation of the complex leaving Cu metal and few sulfur as residues [43].

The thermal decomposition of free H_2L^4 proceeded in three significant thermal events from 70 to 250 °C, 250 to 360 °C, and 360 to 590 °C. The maximum DTG peaks occur at 221, 272, and 453 °C, respectively. The last degradation step accounted for evolution of H_2S and N_2, leaving carbon residue [44]. The TGA/DTG profile of $[Cu(H_2L^4)_2Cl]$ exhibited a thermal degradation behavior different than the other investigated copper complexes

where only one degradation step was demonstrated suggesting the loss of one ligand mole-cule, $C_{14}H_{11}O_4N_3S$, leaving the rest of the complex as a residue up to 1000 °C (scheme S4) (Supplementary Material). This result clearly demonstrated the high thermal stability of [Cu ($H_2L^4)_2$Cl] relative to its analogs. The maximum DTG peak occurs at 300 °C, however, the DTA curve exhibited two endothermic peaks at 225 and 450 °C, in addition to an exother-mic peak at 500 °C.

3.3. *Biological studies*

3.3.1. Antimicrobial activity. The thiourea derivative ligands H_2L^1–H_2L^4 and their Cu(I) complexes were screened against pathogenic bacteria strains *Staphylococcus aurous*, *Bacil-lus subtilis*, and *Micrococcus luteus* (Gram-positive bacteria), *Escherichia coli*, *Pseudomo-nas aeruginosa*, and *Proteus vulgaris* (Gram-negative bacteria) and *Candida albicans* (yeast). Tetracycline and Streptomycin served as standard bacteriocides and Amphotericin B was used as standard fungicide. Screening results are summarized in table 3 and shown in figure 5. The bacterial screening results reveal that H_2L^1 showed the most potent activity against Gram-positive and Gram-negative bacteria. Interestingly, H_2L^1 exhibited significant pronounced activity against *Bacillus subtilis*, *Micrococcus luteus*, and *Proteus vulgaris* strains with growth inhibition zone diameter (46, 32 ,and 31 mm, respectively) greater than the standard bacteriocides in use, tetracycline and streptomycin. In addition, H_2L^2–H_2L^4 showed also a good activity against *Bacillus subtilis* and their activity was found to be in the sequences $H_2L^1 > H_2L^2 > H_2L^4 > H_2L^3$. H_2L^1, and H_2L^2 displayed moderate activity against Gram-positive bacteria *Staphylococcus aureus*, but H_2L^4 showed the least activity, while no activity was detected for H_2L^3. The Gram-negative bacteria screening data showed that H_2L^1 more active against *Proteus vulgaris*, *Escherichia coli*, and *Pseudomonas aeru-ginosa* bacteria while the other ligands showed moderate to low activity against these microbes. From the data given in table 3, it is concluded that the efficacy against Gram-neg-ative bacteria is higher than against Gram positive bacteria. This variation in the activity may be due to the differences in bacteria's cell wall, structure [45] which may be a means to enhance the absorption of various drugs. The anti-yeast activity data revealed that H_2L^1 exert pronounced antifungal activity (inhibition zone diameter 39 mm) compared to the standard fungicide (20 mm). On the contrary, H_2L^3 showed no activity against *Candida albicans*.

Based on the *in vitro* screening results, it is possible to demonstrate structure–property relationship within the investigated ligands. For instance, H_2L^1 has potency as antibacterial and antifungal agent which may be due to *o*-OH that enhances the lipophilicity of the com-pound and allows it to penetrate into the microorganisms. Interestingly, the antimicrobial results of the prepared metal complexes inferred the following observations:

(a) The inhibition zone values observed for the ligands are higher than those found in Cu(I) complexes, except $[Cu(H_2L^2)_2Cl]$ and $[Cu_2L^3)_2Cl] \cdot 2H_2O$, against *Micrococ-cus luteus* and *Proteus vulgaris* strains, and *Escherichia Coli* strains. The results obtained merit notice because it is known that the presence of Cu ions may substan-tially decrease the toxic effect of the ligands [46]. Interestingly, this result matches with that reported for a Ni(II) thiourea complex [40, 47]. The ligand may be more reactive with the microelements present in the medium or the formed complexes may have an uncommon coordination that may be inert to cell constituents. Along

Table 3. Antimicrobial screening results of H_2L^1–H_2L^4 and their copper complexes.

Compound	Inhibition zone diameter (mm/mg sample)						
	Escherichia coli	*Pseudomonas aeruginosa*	*Proteus vulgaris*	*Bacillus subtilis*	*Staphylococcus aureus*	*Micrococcus luteus*	*Candida albicans* (fungus)
H_2L^1	18 ± 0.1	17 ± 0.09	31 ± 0.1	46 ± 0.1	15 ± 0.08	32 ± 0.1	39 ± 0.1
[Cu₂L¹)₂Cl]·2H₂O	0.0 ± 0.0	0.0 ± 0.0	0.0 ± 0.0	0.0 ± 0.0	0.0 ± 0.0	0.0 ± 0.0	15 ± 0.09
H_2L^2	0.0 ± 0.0	0.0 ± 0.0	0.0 ± 0.0	30 ± 0.09	12.0 ± 1.0	0.0 ± 0.0	14 ± 0.10
[Cu(H₂L²)₂Cl]	0.0 ± 0.0	0.0 ± 0.0	11 ± 0.06	0.0 ± 0.0	4.0 ± 1.0	12 ± 0.08	20 ± 0.09
H_2L^3	7.0 ± 0.07	10 ± 0.08	0.0 ± 0.0	20 ± 0.09	0.0 ± 0.0	20 ± 0.1	0.0 ± 0.0
[Cu₂L³)₂Cl]·2H₂O	10 ± 0.10	0.0 ± 0.0	8.0 ± 0.08	12 ± 0.05	12 ± 1.0	9.0 ± 1.3	0.0 ± 0.0
H_2L^4	9.0 ± 0.08	9.0 ± 1.0	6.0 ± 0.1	24 ± 0.08	6.0 ± 1.1	18 ± 0.10	13 ± 0.10
[Cu(H₂L⁴)₂Cl]	7.0 ± 1.0	0.0 ± 0.0	0.0 ± 0.00	14.0 ± 1.0	6.0 ± 008	0.0 ± 0.0	0.0 ± 0.0
Tetracycline	32.0 ± 0.19	33 ± 092	27 ± 0.1	25 ± 0.91	32 ± 0.09	20 ± 0.09	–
Streptomycin	18.0 ± 0.91	17 ± 0.96	19 ± 0.97	22 ± 0.1	23 ± 0.095	16 ± 0.91	–
Amphotericin B	–	–	–	–	–	–	20 ± 0.09
Control: DMSO	0.0 ± 0.0	0.0 ± 0.0	0.0 ± 0.0	0.0 ± 0.0	0.0 ± 0.0	0.0 ± 0.0	0.0 ± 0.0

Note: Each value represents mean of sample ± SD for *n* = 3.

with this explanation, we can conclude that the prepared ligands H_2L^1–H_2L^4 may be more reactive with the microelements necessary for bacterial and fungal nutritions.

(b) [Cu(H$_2$L^2)$_2$Cl] exhibits notable activity against *Micrococcus luteus* (Gram-positive bacteria) and *Proteus vulgaris* (Gram-negative bacteria), while its parent ligand H_2L^2 was inactive against the same microorganisms. Such increased activity of Cu (I) complex can be explained on the basis of Overtone's concept [48]. Accordingly, it may be said that [Cu(H$_2$L^2)$_2$Cl] gave sensitive nature for H_2L^2 against some bacteria and fungi.

(c) The different degrees of antimicrobial activity of copper complexes in relation to the tested species depend either on the impermeability of the cells of the microbes or differences in ribosome in microbial cells [49].

3.3.2. *In vitro* **cytotoxicity screening.** Most investigations in the treatment of cancer are oriented to synthesize new metal complexes analogous to *cis*-diaminodichloroplatinum(II) (cisplatin), but there is a growing number of non-platinum metal complexes which also exhibit remarkable anticancer activities [50, 51]. The preliminary anticancer activities of [Cu(H$_2$L$^{1–4}$)$_2$Cl]·nH$_2$O, $n = 0$ or 2, were evaluated against three human cell lines, liver
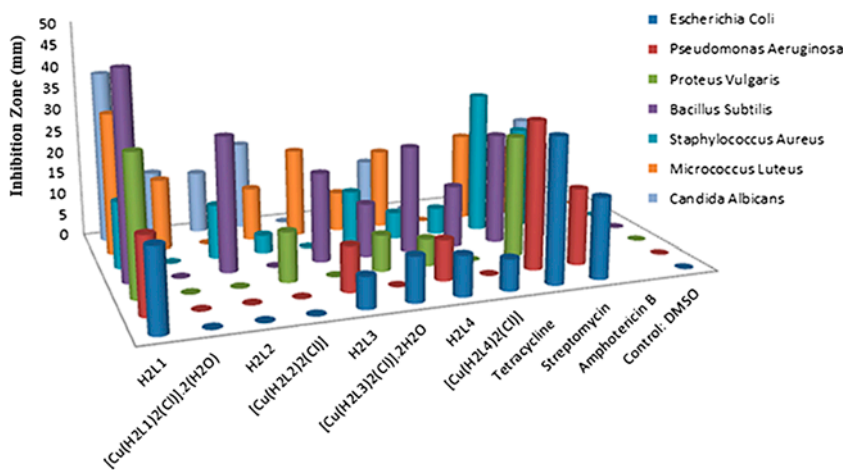
Figure 5.   Antimicrobial activity of H_2L^1–H_2L^4 and their copper complexes.

Table 4.   IC$_{50}$ values (μg/mL) of copper(I) complexes and vinblastine standard drug in HEPG2, MCF7, and HCT116 (doses ranging from 1.56 to 50 μg/mL).

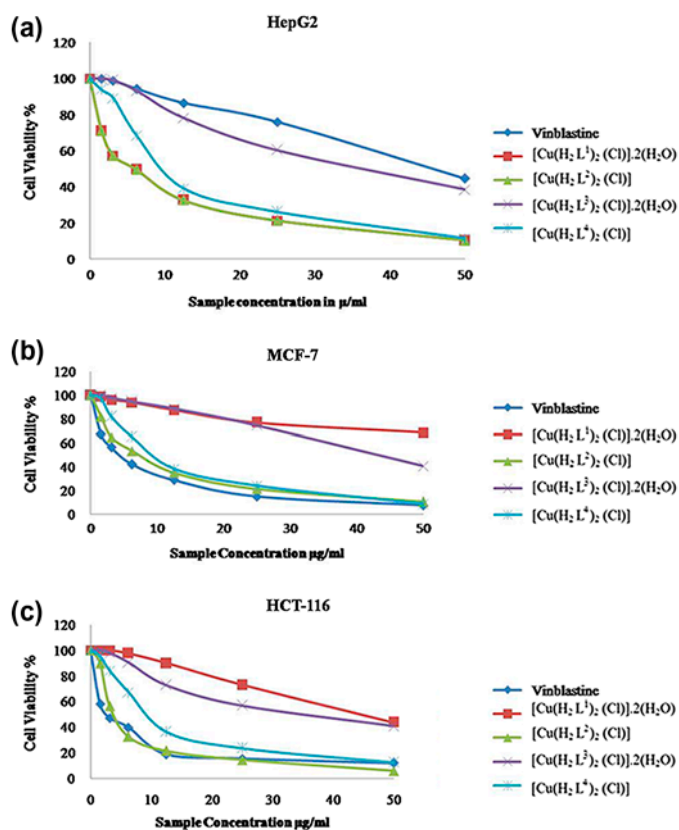| Test compounds	IC$_{50}$ (μg/mL)		
	HEPG2 (liver carcinoma)	MCF7 (breast carcinoma)	HCT116 (colon carcinoma)
[Cu$_2$L^1)$_2$Cl]·2H$_2$O	45.7 ± 2.2	>50.0 ± 2.4	44.7 ± 1.1
[Cu(H$_2$L^2)$_2$Cl]	6.1 ± 0.6	7.4 ± 1.6	4.0 ± 0.3
[Cu$_2$L^3)$_2$Cl]·2H$_2$O	36.8 ± 2.0	43.2 ± 2.2	35.7 ± 0.8
[Cu(H$_2$L^4)$_2$Cl]	10.2 ± 0.4	9.8 ± 7.14	9.7 ± 0.4
Vinblastine	4.6 ± 0.09	4.6 ± 0.8	2.38 ± 0.6

Figure 6. Plot of cell viability % *vs.* increasing of copper complexes concentration against (a) HEPG2, (b) MCF7, and (c) HCT116.

carcinoma (HEPG2), breast carcinoma (MCF7), and colon carcinoma (HCT116). Various concentrations of copper complexes were used to calculate IC_{50} values (IC_{50} corresponds to the concentration required to inhibit 50% of the culture growth when cells are exposed to the tested compounds for 48 h), and vinblastine was used as a reference drug. The screening results are given in table 4 and displayed in figure 6.

All copper complexes exhibited cytotoxicity against the examined cell lines as evident by the range of IC_{50} values (table 4) and the percentage of cell viability. Generally, all the tested compounds tended to be more active against HCT116 than against other cell lines. From the data in hand, it is possible to correlate the activity and the structure change of the N′-phenyl substituent and thus, the investigated copper(I) complexes follow the order [Cu$(H_2L^2)_2$Cl] > [Cu$(H_2L^4)_2$Cl] > [Cu$(H_2L^3)_2$Cl]·2H$_2$O > [Cu$(H_2L^1)_2$Cl]·2H$_2$O. [Cu$(H_2L^2)_2$Cl] showed the highest potency against the tested cell lines with IC_{50}, 4.0, 6.1, and 7.4 μg/mL, respectively, for colon carcinoma HCT116, breast carcinoma MCF7, and liver carcinoma HEPG2; [Cu$(H_2L^1)_2$Cl]·2H$_2$O exhibited the lowest activity.

Table 5. Statistical analyses of IC_{50} values (µg/mL) of copper complexes against HEPG2, MCF7, and HCT116.

	$[Cu(H_2L^1)_2Cl]\cdot2H_2O$	$[Cu(H_2L^2)_2Cl]$	$[Cu(H_2L^3)_2Cl]\cdot2H_2O$	$[Cu(H_2L^4)_2Cl]$	F (p)
HEPG2 (liver carcinoma)	45.7 ± 2.2	6.1 ± 0.6	36.8 ± 2.0	10.2 ± 0.4	488.726^* ($<0.001^*$)
p_1		$<0.001^*$	0.009^*	$<0.001^*$	
p_2			$<0.001^*$	0.001^*	
p_3			$<0.001^*$		
MCF7 (breast carcinoma)	$>50.0 \pm 2.4$	7.4 ± 1.6	43.2 ± 2.2	9.8 ± 7.14	91.675^* ($<0.001^*$)
p_1		$<0.001^*$	0.022^*	0.001^*	
p_2			$<0.001^*$	0.600	
p_3			0.002^*		
HCT116 (colon carcinoma)	44.7 ± 1.1	4.0 ± 0.3	35.7 ± 0.8	9.7 ± 0.4	226.605^* ($<0.001^*$)
p_1		$<0.001^*$	0.001^*	$<0.001^*$	
p_2			$<0.001^*$	$<0.001^*$	
p_3			$<0.001^*$		

Notes: Data were expressed using mean ± SD.
F: F test (ANOVA).
p_1: p value for Post Hoc test (LSD) for comparing between $[Cu(H_2L^1)_2Cl]\cdot2H_2O$ and other copper complexes.
p_2: p value for Post Hoc test (LSD) for comparing between $[Cu(H_2L^2)_2Cl]$ and other copper complexes.
p_3: p value for Post Hoc test (LSD) for comparing between $[Cu(H_2L^3)_2Cl]\cdot2H_2O$ and $[Cu(H_2L^4)_2Cl]$.
*Statistically significant at $p \leq 0.05$.

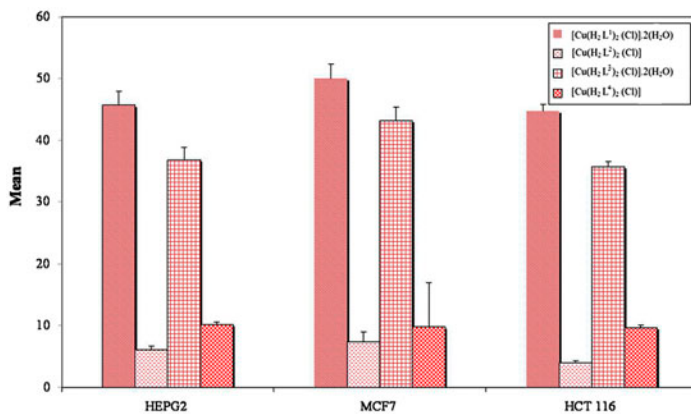Figure 7. IC_{50} values of the investigated copper(I) complexes against HEPG2, MCF7, and HCT116.

3.3.3. Statistical analysis of the data. *In vitro*, cytotoxicity data were analyzed using SPSS software package version 18.0 (SPSS, Chicago, IL, USA) (table 5, figure 7). Details of data analysis using an *F*-test (ANOVA) to compare the three categories of outcome are provided as Supplementary Material.

4. Conclusion

Four copper complexes were synthesized from nanosized isomeric *N*-benzoyl-*N'*-(hydroxy-phenyl) thioureas H_2L^1–H_2L^4. Analytical, spectroscopic, and thermal data proved the formation of non-electrolytic mononuclear three-coordinate copper(I) complexes, where the ligands are hypodentate, bonded to copper ion via their thioamide sulfur. The *N*-benzoyl-*N'*-(*o*-hydroxyphenyl) thiourea, H_2L^1, exhibited significant antimicrobial effect compared to the standard fungicides and bacteriocides in use. $[Cu(H_2L^2)_2Cl]$ showed potency as antitumor agent against the tested cell lines. The bioactivity results in this study clearly indicate that the lipophilic nature corresponds to structural change of the *N'*-phenyl substituent in membrane binding and facilitates drug penetration within the infected cells.

References

[1] B. Akermark, J. Bjernemose, A. Borje, P.J. Chmielewski, H. Paulsen, O. Simonsen, P.C. Stein, H. Toftlund, J.A. Wolny. *Dalton Trans.*, 1215, (2004).
[2] A. Molter, F. Mohr. *Coord. Chem. Rev.*, **254**, 19 (2010).
[3] R. Richter, J. Sieler, L. Beyer, O. Lindqvist, L.Z. Anderson. *Anorg. Allg. Chem.*, **522**, 183 (1985).
[4] A.N. Westra, C. Esterhuysen, K.R. Koch. *Acta Crystallogr.*, **C60**, m395 (2004).
[5] M.A. Arif, B.M. Yamin. *Acta Crystallogr.*, **E63**, 03594 (2007).
[6] B.Q. Su, L. Xian, H.B. Song, L. Sheng. *Acta Crystallogr.*, **C60**, m661 (2004).
[7] J. Černák, J. Chomič, P. Kutschy, D. Svrčinová, M. Dzurilla. *Inorg. Chim. Acta*, **181**, 85 (1991).
[8] M.M. Habtu, S.A. Bourne, K.R. Koch, R.C. Luckay. *New J. Chem.*, **30**, 1155 (2006).
[9] J.C. Bruce, N. Revaprasadu, K.R. Koch. *New J. Chem.*, **31**, 1647 (2007).
[10] N. Selvakumaran, S.W. Ng, E.R.T. Tiekink, R. Karvembu. *Inorg. Chim. Acta*, **376**, 278 (2011).
[11] W.H. Du, C.M. Wei, W.F. Wang. *Acta Crystallogr.*, **E65**, o308 (2009) and references therein.
[12] M.S.M. Yusof, R.H. Jusoh, W.M. Khairul, B.M. Yamin. *J. Mol. Struct.*, **975**, 280 (2010).
[13] P.A. Gale, S.E. García-Garrido. *J. Garric. Chem. Soc. Rev.*, **37**, 151 (2007).
[14] R.C. Luckay, F. Mebrahtu, C. Esterhuysen, K.R. Koch. *Inorg. Chem. Commun.*, **13**, 468 (2010).
[15] M.P. Sibi, K. Itoh. *J. Am. Chem. Soc.*, **129**, 8064 (2007).
[16] K.G. Daniel, D. Chen, S. Orlu, Q.C. Cui, F.R. Miller, Q.P. Dou. *Breast Cancer Res.*, **7**, R897 (2005).
[17] G. Murtaza, M.K. Rauf, A. Badshah, M. Ebihara, M. Said, M. Gielen, D. de Vos, E. Dilshad, B. Mirza. *Eur. J. Med. Chem.*, **48**, 26 (2012).
[18] U. El-Ayaan. *J. Mol. Struct.*, **998**, 11 (2011).
[19] G.J. Brewer. *Exp. Biol. Med. (Maywood)*, **226**, 665 (2001).
[20] S. Brem. *Cancer Control*, **6**, 436 (1999).
[21] K.G. Daniel, P. Gupta, R.H. Harbach, W.C. Guida, Q.P. Dou. *Biochem. Pharmacol.*, **67**, 1139 (2004).
[22] H.M. Abosadiya, B.M. Yamin, N. Ngah. *Acta Cryst.*, **E63**, o2403 (2007).
[23] A. Al-abbasi, S.S. Tan, M.B. Kassim. *Acta Cryst.*, **E66**, o3181 (2010).
[24] (a) J.P. Rao, K.E. Geckeler. *Prog. Polym. Sci.* **36**, 887 (2011); (b) C. Burda, X. Chen, R. Narayanan, M.A. El-Sayed. *Chem. Rev.* **105**, 1025 (2005).
[25] A.A.A. Emara, M.A. Tawab, M.A. El-ghamry, M.Z. Elsabee. *Carbohydr. Polym.*, **83**, 192 (2011).
[26] T. Mosmann. *J. Immunol. Methods*, **65**, 55 (1983).
[27] P. Vijayan, C. Raghu, G. Ashok, S.A. Dhanaraj, B. Suresh. *Indian. J. Med. Res.*, **120**, 24 (2004).
[28] A.W. Bauer, W.M. Kirby, C. Sherris, M. Turck. *Am. J. Clinic Path.*, **45**, 493 (1966).
[29] S.M. Finegold, W.J. Martin. *Diagnostic Microbiology*, 6th Edn, Louis S, London (1982).
[30] H. Fessi, F. Puisieux, J.P. Devissaguet, N. Ammoury, S. Benita. *Int. J. Pharm.*, **55**, R1 (1989).
[31] (a) I. Limayem Blouza, C. Charcosset, S. Sfar, H. Fessi. *Int. J. Pharm.*, **325**, 124 (2006); (b) V. Ferranti, H. Marchais, C. Chabenat, A.M. Orecchioni, O. Lafont. *Int. J. Pharm.*, **193**, 107 (1999).
[32] F. Lince, D.L. Marchisio, A.A. Barresi. *J. Colloid Interface Sci.*, **322**, 505 (2008).
[33] S. Sahu, P. Rani Sahoo, S. Patel, B.K. Mishra. *J. Sulfur Chem.*, **32**, 171 (2011) and references therein.
[34] Y.F. Yuan, J.T. Wang, M.C. Gimeno, A. Laguna, P.G. Jones. *Inorg. Chim. Acta*, **324**, 309 (2001).
[35] A. Saeed, M.F. Erben, M. Bolte. *Spectrochim. Acta*, **102**, 408 (2013).
[36] B.M. Yamin, S. Yousuf, M.S.M. Yusof, R.H. Jusoh. *Acta Crystallogr.*, **E64**, O832 (2008).
[37] G. Binzet, F.M. Emen, U. Flörke, T. Yesilkaynak, N. Külcü, H. Arslan. *Acta Crystallogr.*, **E65**, O81 (2009).
[38] H.M. Badawi. *Spectrochim. Acta*, **72**, 523 (2009).
[39] F. Karipcin, M. Atis, B. Sariboga, H. Celik, M. Tas. *J. Mol. Struct.*, **1048**, 69 (2013).

[40] M.K. Rauf, I. Imtiaz-ud-Din, A. Badshah, M. Gielen, M. Ebihara, D. Vos, S. Ahmed. *J. Inorg. Biochem.*, **103**, 1135 (2009).
[41] S. Singhal, A.N. Garg, K. Chandra. *J. Alloys Compd.*, **428**, 72 (2007).
[42] M.J. Moloto, M.A. Malik, P. O'Brien, M. Motevalli, G.A. Kolawole. *Polyhedron*, **22**, 595 (2003).
[43] D.C. Onwudiwe, P.A. Ajibade. *Int. J. Mol. Sci.*, **13**, 9502 (2012).
[44] W.M.I. Hassan, M.A. Badawy, G.G. Mohamed, H. Moustafa, S. Elramly. *Spectrochim. Acta*, **111**, 169 (2013).
[45] D. Quintanar-Guerrero, E. Allémann, H. Fessi, E. Doelker. *Pharm. Res.*, **14**, 119 (1997).
[46] J.R.J. Sorenson. *Inflammatory Diseases and Copper*, Humana Press, Clifton (1982).
[47] H. Arslan, N. Duran, G. Borekci, C. Koray Ozer, C. Akbay. *Molecules*, **14**, 519 (2009).
[48] S.J. Lippard, J.M. Berg. *Principles of Bioorganic Chemistry*, University Science Book, Mill Valley (1994).
[49] Z.H. Chohan. *Appl. Organomet. Chem.*, **20**, 112 (2006).
[50] B. Rosenberg. *Metal Ions in Biological Systems*, **II**, 127, New York (1980).
[51] T. Hambley. *Coord. Chem. Rev.*, **166**, 181 (1997).